Check for updates

Nf1 deficiency modulates the stromal environment in the pretumorigenic rat mammary gland

Menusha Arumugam[1†], Elizabeth A. Tovar[1], Curt J. Essenburg[1], Patrick S. Dischinger[1], Ian Beddows[2], Emily Wolfrum[2], Zach B. Madaj[2], Lisa Turner[3], Kristin Feenstra[3], Kristin L. Gallik[4], Lorna Cohen[4], Madison Nichols[5], Rachel T. C. Sheridan[5], Corinne R. Esquibel[4], Ghassan Mouneimne[6,7], Carrie R. Graveel[1‡]* and Matthew R. Steensma[1,8,9‡]*

[1]Department of Cell Biology, Van Andel Research Institute, Grand Rapids, MI, United States, [2]Biostatistics ad Bioinformatics Core, Van Andel Research Institute, Grand Rapids, MI, United States, [3]Pathology and Biorepository Core, Van Andel Research Institute, Grand Rapids, MI, United States, [4]Optical Imaging Core, Van Andel Research Institute, Grand Rapids, MI, United States, [5]Flow Cytometry Core, Van Andel Research Institute, Grand Rapids, MI, United States, [6]University of Arizona Cancer Center, Tucson, AZ, United States, [7]Department of Cellular and Molecular Medicine, University of Arizona, Tucson, AZ, United States, [8]Helen DeVos Children's Hospital, Spectrum Health System, Grand Rapids, MI, United States, [9]Michigan State University College of Human Medicine, Grand Rapids, MI, United States

Background: Neurofibromin, coded by the *NF1* tumor suppressor gene, is the main negative regulator of the RAS pathway and is frequently mutated in various cancers. Women with Neurofibromatosis Type I (NF1)—a tumor predisposition syndrome caused by a germline *NF1* mutation—have an increased risk of developing aggressive breast cancer with poorer prognosis. The mechanism by which *NF1* mutations lead to breast cancer tumorigenesis is not well understood. Therefore, the objective of this work was to identify stromal alterations before tumor formation that result in the increased risk and poorer outcome seen among NF1 patients with breast cancer.

Approach: To accurately model the germline monoallelic *NF1* mutations in NF1 patients, we utilized an *Nf1*-deficient rat model with accelerated mammary development before presenting with highly penetrant breast cancer.

Results: We identified increased collagen content in *Nf1*-deficient rat mammary glands before tumor formation that correlated with age of tumor onset. Additionally, gene expression analysis revealed that *Nf1*-deficient mature adipocytes in the rat mammary gland have increased collagen expression and shifted to a fibroblast and preadipocyte expression profile. This alteration in lineage commitment was also observed with *in vitro* differentiation, however, flow cytometry analysis did not show a change in mammary adipose-derived mesenchymal stem cell abundance.

Conclusion: Collectively, this study uncovered the previously undescribed role of *Nf1* in mammary collagen deposition and regulating adipocyte differentiation. In addition to unraveling the mechanism of tumor formation, further investigation of

adipocytes and collagen modifications in preneoplastic mammary glands will create a foundation for developing early detection strategies of breast cancer among NF1 patients.
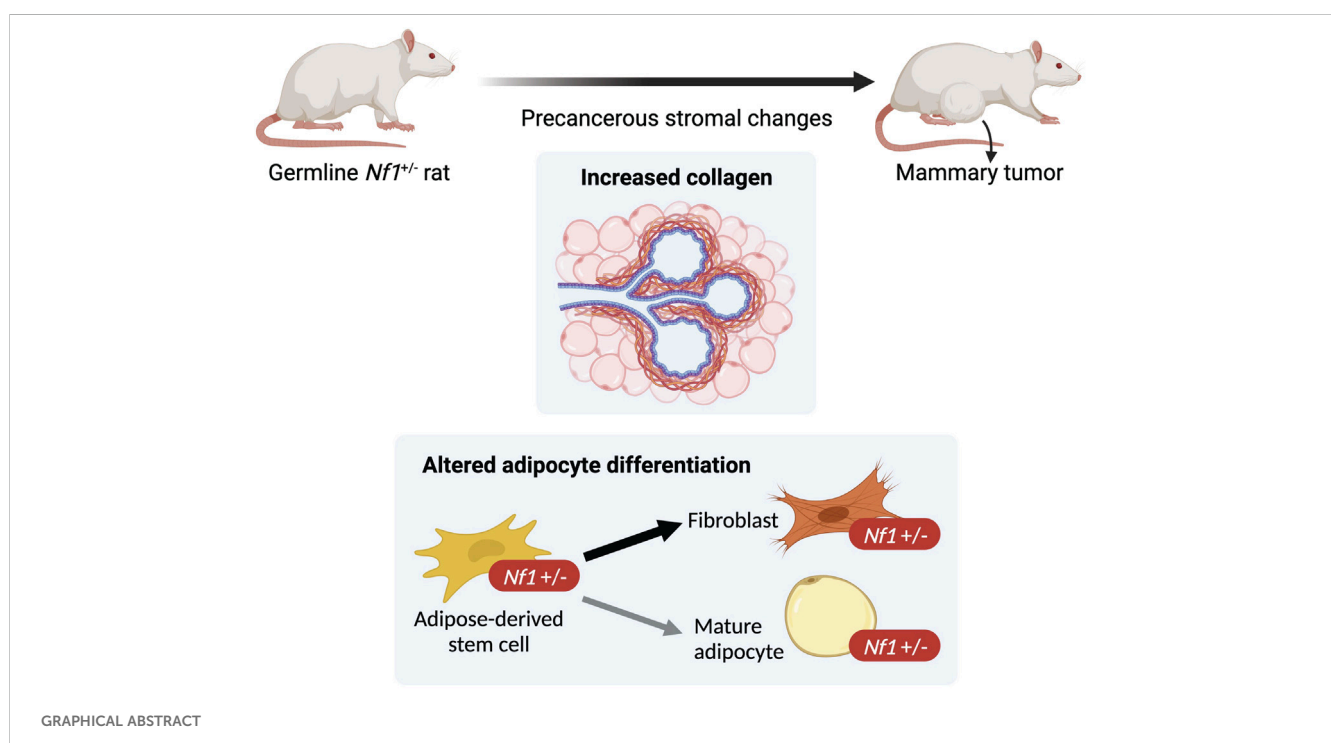
1 Introduction

The tumor suppressor gene Neurofibromin 1 (*NF1*) codes for the protein neurofibromin and is the main negative regulator of the RAS pathway. Loss-of-function or genomic alterations in *NF1* result in dysregulated RAS signaling, including the MAPK (mitogen-activated protein kinase) pathway (Xu et al., 1990; Yap et al., 2014; Ratner and Miller, 2015). The role of *NF1* has been commonly studied in the context of Neurofibromatosis type 1 (NF1), a tumor predisposition syndrome affecting one in 3,000 live births caused by mutations in the *NF1* gene (Rasmussen and Friedman, 2000; Lammert et al., 2005; Griffiths et al., 2007; Evans et al., 2010; Yap et al., 2014; Mo et al., 2022). While benign and malignant tumors of the nervous system are the more common clinical manifestation of NF1, several recent studies have identified *NF1* as a genetic driver of both sporadic and inherited breast cancer (Comprehensive molecular portraits of human, 2012; Stephens et al., 2012). These studies revealed that women with NF1 have a 5-7-fold increased risk of developing breast cancer at a younger age (Madanikia et al., 2012; Wang et al., 2012; Seminog and Goldacre, 2015; Uusitalo et al., 2016; Uusitalo et al., 2017; Landry et al., 2021). This elevated risk has warranted the recommendation for earlier breast cancer screening at the age

of 30 for women with NF1 (Sharif et al., 2007; Daly et al., 2017). NF1-related breast cancers are associated with adverse prognostic factors, aggressive molecular subtypes (HER2+ and triple-negative breast cancers), and decreased overall survival compared to sporadic breast cancer (Uusitalo et al., 2017). Additionally, our analysis of the METABRIC breast cancer dataset showed that patients with *NF1* shallow deletions are 1.65 times more likely to die within the first 10 years compared to patients with diploid *NF1* status (Dischinger et al., 2018). *NF1* loss of function is also more commonly detected in endocrine-resistant and metastatic breast cancer cases (Meric-Bernstam et al., 2014; Yates et al., 2017; Razavi et al., 2018; Bertucci et al., 2019; Sokol et al., 2019; Pearson et al., 2020). Despite this clear role of NF1 in sporadic and inherited breast cancer, the molecular mechanisms of *NF1*-mediated breast cancer formation are still poorly understood.

To address this question, we developed a rat model of *Nf1*-deficient breast cancer by creating several distinct germline *Nf1* indels using CRISPR/Cas9 genome editing in immunocompetent Sprague Dawley rats (Dischinger et al., 2018). All of these indels model "*Nf1* deficiency" and induce highly penetrant, aggressive ER+/PR + mammary adenocarcinomas in female rats. In our studies of tumor initiation and progression, we observed that these aggressive tumors could not be transplanted into *Nf1*⁺/⁺ Sprague-Dawley or Athymic nude rats. The

Germline *Nf1*⁺/⁻ rat

Precancerous stromal changes

Mammary tumor

Increased collagen

Altered adipocyte differentiation

Adipose-derived stem cell

Nf1 +/-

Fibroblast

Nf1 +/-

Mature adipocyte

Nf1 +/-

GRAPHICAL ABSTRACT

FIGURE 1
Nf1-deficient rat breast cancer lines have increased matrix before tumor formation. **(A)** Schematic of indels generated in one copy of the *Nf1* gene in immunocompetent Sprague Dawley rats resulting in three *Nf1* mutant lines: *Nf1* in frame (IF/+), premature stop-20 (PS-20/+), as well as in-frame and premature stop-21 (IF; PS-21/+). **(B)** Tumor onset in *Nf1*-deficient rats. All animals in this study died of mammary tumor progression. Representative H&E images and eosin quantification of rat mammary gland at **(C)** 21 and **(D)** 33 days. **(E)** Representative brightfield and polarized microscopy images of picrosirius red (PSR)-stained rat mammary glands at 43 days, and quantification of polarized light signal. Each data point represents a tissue from an individual rat as a biological replicate.

results of these transplantation experiments indicated that an *Nf1*-deficient mammary stroma was necessary to promote tumor growth and progression. Therefore, this led us to question the role of *Nf1* in stromal cells and how *Nf1*-deficiency alters the mammary stroma in our rat model.

The mammary gland is composed of epithelial ducts surrounded by stromal cells such as fibroblasts, adipocytes, endothelial cells, and immune cells embedded in a complex web of extracellular matrix (ECM). Although breast cancer arises from the epithelial cells, numerous studies have

demonstrated the significant impact of the stroma on the earliest stages of tumor initiation, tumor progression, metastasis, and even clinical outcome (Finak et al., 2008; Oh et al., 2015; Bainer et al., 2016; de Visser and Joyce, 2023; Curran and Ponik, 2022). Adipocytes make up a significant majority of the stromal cell population and can dedifferentiate to become preadipocytes/mesenchymal-like cells during mammary gland remodeling through a process called adipocyte mesenchymal transition (AMT), which consequently also creates a tumor-promoting environment (Zhu et al., 2022). In the tumor microenvironment, adipocytes are pushed into an activated state known as a cancer-associated adipocyte (CAA) (Dirat et al., 2011; Zhang et al., 2012; Bochet et al., 2013; Attane and Muller, 2020; Mukherjee et al., 2022; Wu et al., 2023), resulting in protumorgenic metabolic reprogramming and increased collagen secretion (Bi et al., 2016; Wang et al., 2017; Wei et al., 2019). Overall, these findings highlight the plasticity of adipocytes in both normal and cancerous mammary glands.

In our study, we investigated the impact of *Nf1* loss of function on the mammary stroma before tumor formation. Studies on epithelial cells of NF1-related breast cancer has expanded our knowledge of their direct tumorigenic mechanisms (Dischinger et al., 2018; Zheng et al., 2020; Tovar et al., 2022), but there remains a gap in our understanding of the impact of *NF1* on the mammary stroma. The preneoplastic stromal alternations of inherited cancer syndromes have also been recently characterized in the context of individuals with germline BRCA1 mutations. This study identified a population of BRCA$^{+/mut}$ fibroblast present before cancer formation that increased epithelial proliferation, altered epithelial differentiation, and promoted BRCA1-driven tumorigenesis *in vivo* (Nee et al., 2023). Since individuals with NF1 also have germline *NF1* mutations in both stromal and epithelial cells, these results naturally raise the important question of whether *NF1*-deficient stromal cells provide a protumorigenic niche for epithelial transformation and contribute to the increased risk of breast cancer in individuals with NF1. Here, we demonstrate that *Nf1*-deficient rat mammary glands have increased collagen deposition in their pretumorigenic glands. We observed increased expression of collagen and ECM genes specifically in adipocytes that were in a dedifferentiated preadipocyte/fibroblast-like state. Additionally, *Nf1*-deficient adipose-derived stem cells (ASC) also had a decreased adipogenic differentiation capacity. Together, our findings demonstrate that *Nf1* alters pretumorigenic mammary stroma by increasing collagen deposition and disrupting adipocyte differentiation.

2 Results

2.1 Nf1-deficiency results in increased matrix deposition before mammary tumor initiation

To investigate the role of *Nf1* in the mammary tumorigenesis, we previously generated three mutant lines representing distinct states of *Nf1* deficiency (Figure 1A). (Dischinger et al., 2018) In this model, we targeted exons 21–22 (previously denoted as exons 20–21) within the CSRD (cysteine-serine rich domain) of *Nf1*.

The CSRD is an allosteric activator of the adjacent GRD (GAP-related domain) and near the dimerization region of neurofibromin (Lupton et al., 2021; Young et al., 2023). Recent studies have revealed that hotspot mutations in the CSRD region lead to severe phenotypes in NF1 individuals (Koczkowska et al., 2018; Koczkowska et al., 2020). The IF/+ animals harbor an in-frame indel in exon 21, whereas the PS/+ rats have a premature stop codon in exon 21. The IF; PS-21/+ line was derived from an in-frame indel in exon 21 (previously exon 20) and a distinct mRNA isoform with a premature stop in exon 22 (previously exon 21). By creating indels in the CSRD of one copy of the *Nf1* gene, each of these *Nf1*-deficient immunocompetent rat lines developed highly penetrant, aggressive mammary adenocarcinomas with varying times on tumor onset. The IF/+ line, with the least impact on neurofibromin function, had the slowest tumor onset, the PS-20/+ and IF; PS-21/+ lines with a premature stop indel (thus removing all the domains after the CSRD) resulted in animals with quicker tumor onset (Figure 1B). The difference in tumor initiation between the *Nf1* indels offers distinct models in which to study the pretumorigenic changes, with a long window of before tumor onset in IF/+ rats compared to the rapid tumor onset that occurs in the PS-20/+ and IF; PS-21/+ lines.

To understand the mechanism of different tumor onset, it is vital to understand the changes that occur in preneoplastic glands that create an environment of tumor permissiveness. While we have previously shown an increase in mammary epithelial branching and end bud formation during development (Tovar et al., 2022), H&E staining also shows an increased matrix region around the mammary ducts and end buds of *Nf1* deficient rats compared to WT. To quantify this difference, we measured the percent area of eosin around the ducts. At 21 days, the odds of having eosin staining are 14 times higher in *Nf1*-deficient IF; PS-21/+ tissue than WT tissues ($p = 0.005$, Figure 1C). However, at 33 days, the odds of having eosin staining in *Nf1*-deficient PS-20/+ and IF; PS-21/+ tissues are 5 times ($p = 0.002$) and 8 times ($p < 0.001$) higher respectively compared to WT tissues (Figure 1D). At both 21 and 33 days, the odds of having more eosin staining in *Nf1*-deficient IF/+ tissues than WT tissues are not statistically significant with the odds of having more eosin staining only 2 times higher odds ($p = 0.619$ at 21 days; $p = 0.959$ at 33 days).

To verify that this increase in eosin correlates with an increase in collagen deposition that progresses with age towards tumor formation, we stained tissues from 43-day-old rats with picrosirius red (PSR) that allows for collagen visualization under exposure of polarized light (Coelho et al., 2018). At 43 days, all *Nf1*-deficient mammary glands had increased collagen content compared to the WT glands. Consistent with the eosin quantification, both *Nf1*-deficient PS-20/+ and IF; PS-21/+ tissues showed approximately 150% increase in polarized light (POL) signals compared to the WT tissues ($p < 0.01$; Figure 1E). Interestingly, although still lower than the other two *Nf1*-deficient genotypes, the IF/+ tissues at 43 days also had an increase in POL signals as well, about 72% more than the WT tissues ($p = 0.02$; Figure 1E). This increase in collagen indicates that as the IF/+ rats approach an age closer to tumor formation, their collagen content also increases.
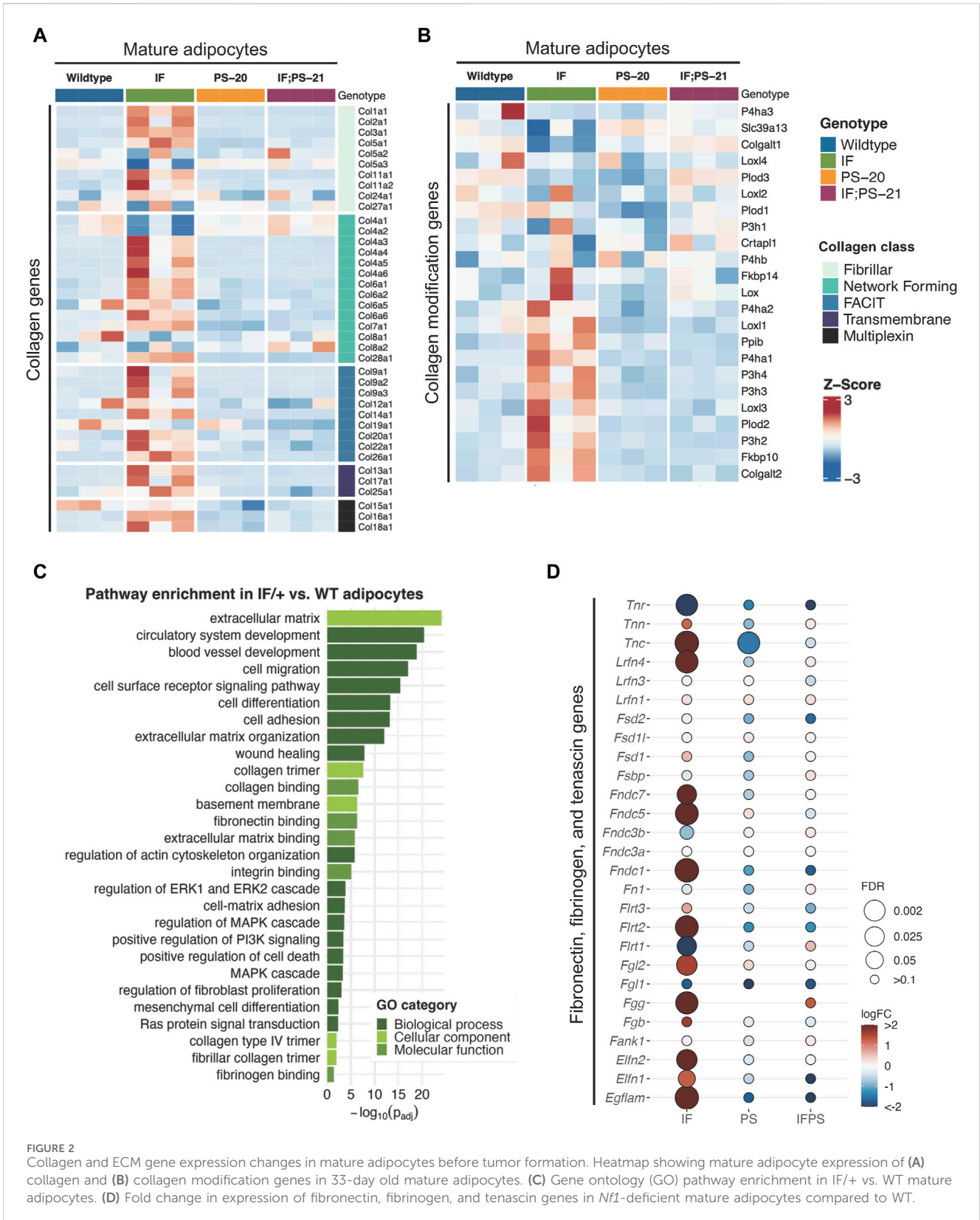
FIGURE 2
Collagen and ECM gene expression changes in mature adipocytes before tumor formation. Heatmap showing mature adipocyte expression of **(A)** collagen and **(B)** collagen modification genes in 33-day old mature adipocytes. **(C)** Gene ontology (GO) pathway enrichment in IF/+ vs. WT mature adipocytes. **(D)** Fold change in expression of fibronectin, fibrinogen, and tenascin genes in *Nf1*-deficient mature adipocytes compared to WT.

This indicates that collagen and matrix changes correspond to *Nf1* loss of function and rates of tumor onset. In our model, increases in collagen deposition are present earlier in PS-20/+ and IF; PS-21/+

mammary glands which have a larger loss of neurofibromin and earlier tumor onset (6–12 weeks). In contrast, increase in collagen changes are first observed at 43 days, in IF/+ mammary glands that
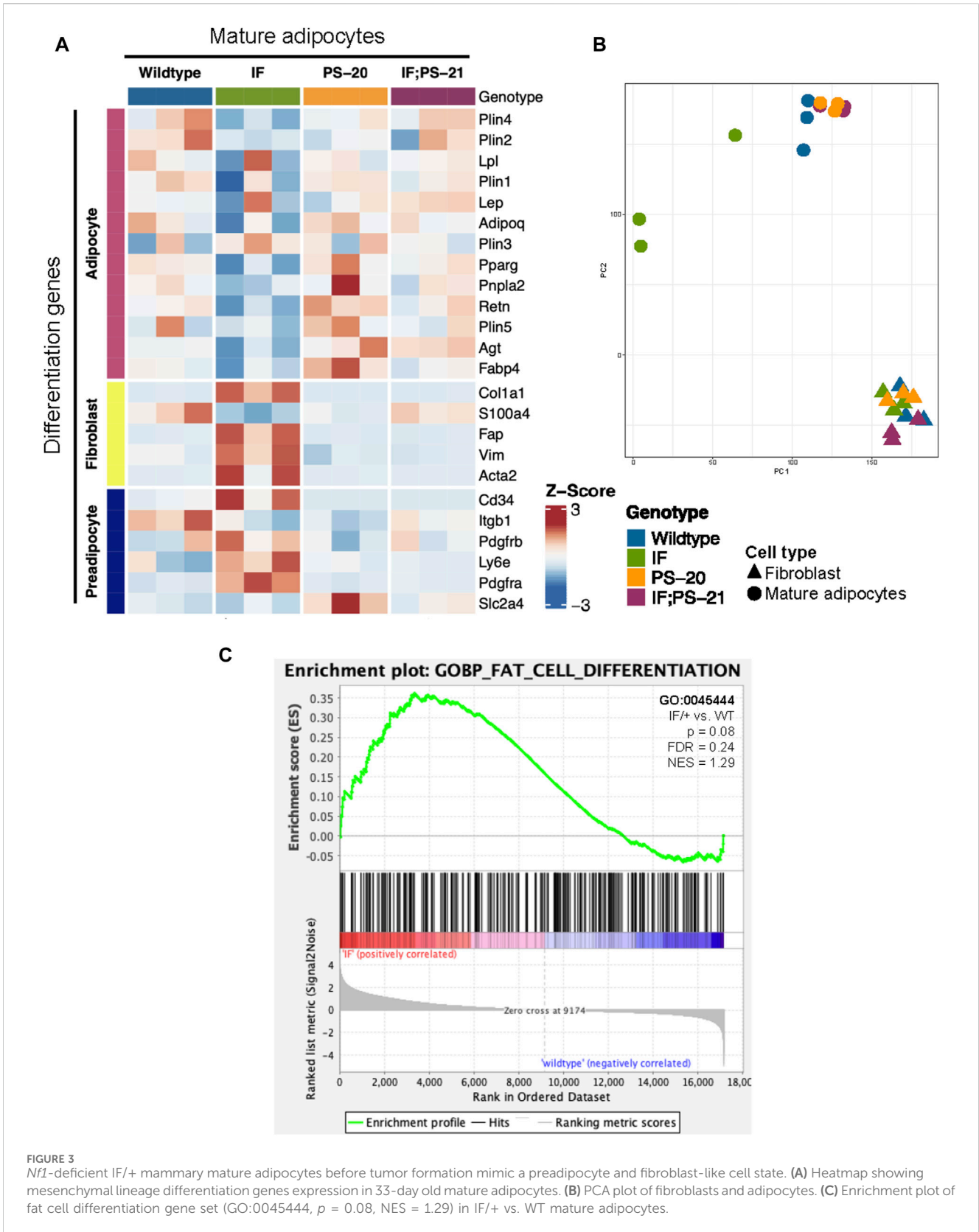
FIGURE 3
Nf1-deficient IF/+ mammary mature adipocytes before tumor formation mimic a preadipocyte and fibroblast-like cell state. **(A)** Heatmap showing mesenchymal lineage differentiation genes expression in 33-day old mature adipocytes. **(B)** PCA plot of fibroblasts and adipocytes. **(C)** Enrichment plot of fat cell differentiation gene set (GO:0045444, *p* = 0.08, NES = 1.29) in IF/+ vs. WT mature adipocytes.

have a minor alteration in neurofibromin and a much later tumor onset (<10 months). These results show that the timing of increase in collagen mirrors the timing of tumor onset in the *Nf1*-deficient lines.

Additionally, to delineate whether the collagen deposition increased solely as a result of epithelial ductal development, we measured fibrosis in mammary glands of older IF/+ rats that did not develop palpable tumors at 7.5 months old. Interestingly, we

discovered a noticeable increase in fibrotic region around epithelial ducts that appear to have ductal carcinoma *in situ* (DCIS; Supplementary Figure S1). We are unable to measure collagen content at later timepoints in PS-20/+ and IF; PS-21/+ lines because they develop mammary adenocarcinomas with complete penetrance by 14 weeks of age. However, in the slower progressing IF/+ line, increased collagen content does persist past the epithelial gland developmental stage into adulthood. This finding underscores the impact of *Nf1* loss of function in remodeling the rat mammary stroma during both pubertal development and adulthood.

2.2 *Nf1*-deficient IF/+ mammary mature adipocytes have increase collagen and ECM genes expression before tumor formation

To identify which cell population and what type of collagen was predominantly involved in the elevated collagen levels, we performed RNAseq of adipocytes, fibroblasts and epithelial cells isolated from mammary glands before tumor formation. Unsupervised clustering of collagen gene expression revealed that each sample expresses different types of collagens with very little overlap between each other (Supplementary Figure S2). As expected, fibroblasts have the highest expression of fibrillar collagens, such as collagen I, III, and V, yet there were no significant differences between the *Nf1*-deficient and WT fibroblasts. Epithelial cells and mature adipocytes primarily express distinct subunits of network forming collagens. Surprisingly, we observed that the *Nf1*-deficient IF/+ mature adipocytes have increased gene expression of collagens (Figure 2A). Because adipocytes are more well known for their endocrine and metabolic functions, we were intrigued by these unexpected findings.

Recent studies have revealed that adipocytes surrounding a tumor can become activated to form cancer-associated adipocytes (CAAs) and have increased collagen secretion (Dirat et al., 2011; Zhang et al., 2012; Bochet et al., 2013; Wei et al., 2019; Zhu et al., 2022). Since the adipocytes we analyzed are from mammary glands before tumor formation, these results indicate that *Nf1* plays a role in normal mammary adipocyte differentiation. Next, we examined whether the IF/+ mature adipocytes also exhibit other reported gene expression features of CAAs. Along with increased collagen secretion, these studies also reported that CAAs can remodel collagen architecture and alignment through increased expression of collagen modification genes (Wei et al., 2019). An example of a collagen modification gene is prolyl 4-hydroxylase subunit alpha 1 (*P4ha1*), which is the most important catalytic subunit of the P4H enzyme and necessary for collagen polypeptide chains folding into stable triple-helical molecules (Myllyharju and Kivirikko, 2004). From our RNAseq data, *P4ha1* and other collagen modification genes have increased expression in IF/+ mature adipocytes compared to the WT and two other *Nf1*-deficient mature adipocytes (Figure 2B). Additionally, gene ontology (GO) analysis of *Nf1*-deficient IF/+ mature adipocytes gene expression compared to WT showed enrichment in pathways involved in ECM processes and RAS-MAPK signaling (Figure 2C). Pathways involved in MAPK signaling were expected due to neurofibromin's role as a negative regulator of RAS. Enrichment of pathways in ECM
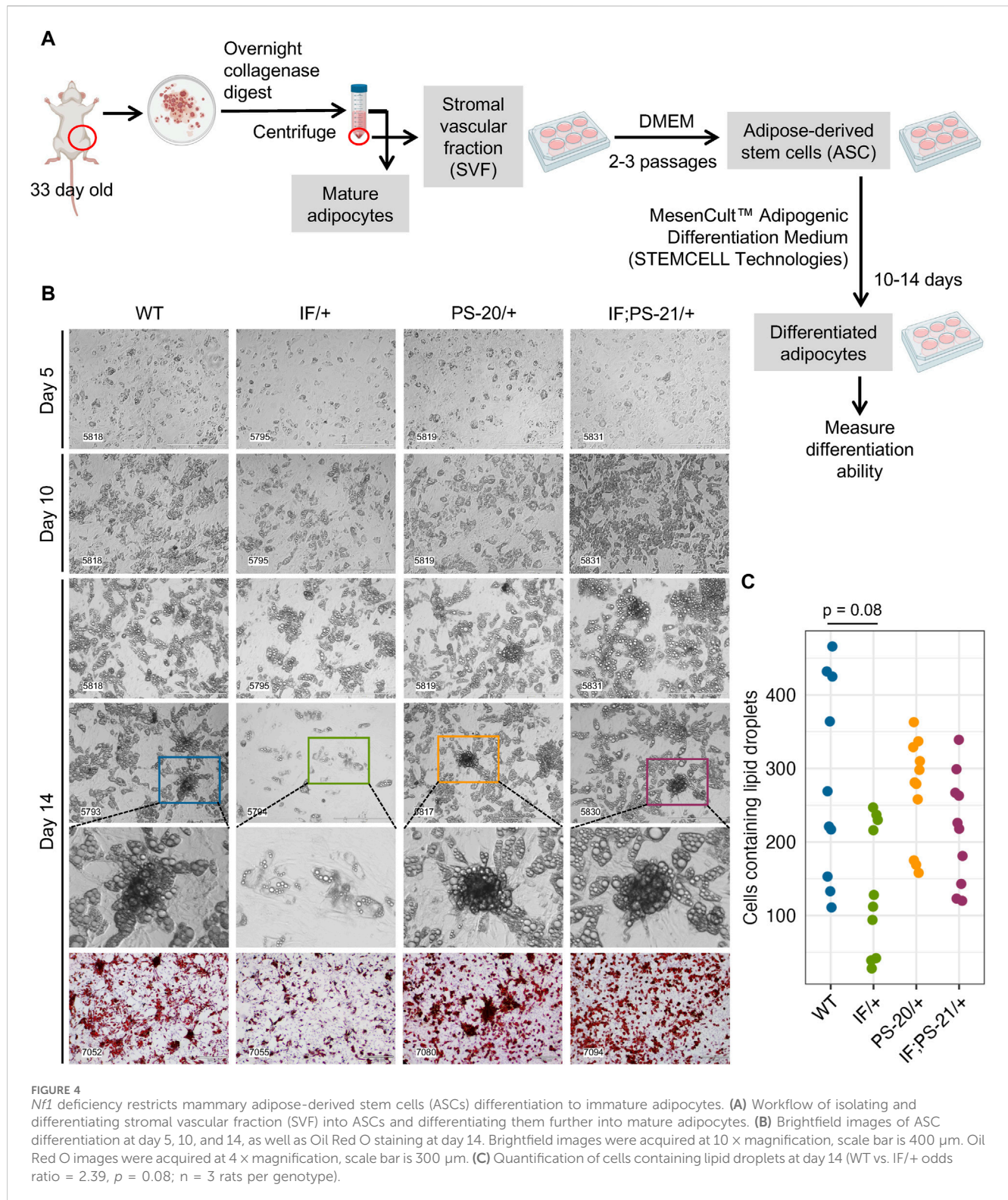
processes substantiates a role for *Nf1*-deficient IF/+ adipocytes in collagen deposition and a CAA-like phenotypes (Figures 2A, B). Our analysis indicated other ECM components besides collagen may contribute to tumorigenesis in *Nf1*-deficient IF/+ glands. Several genes typically known for their role in tissue fibrosis (i.e., tenascin, fibrinogen, and fibronectin genes) were increased in *Nf1*-deficient IF/+ adipocytes (Figure 2D). Overall, these results demonstrated that *Nf1*-deficient IF/+ adipocytes have increased collagen and fibrosis-related ECM gene expression preceding tumor formation.

2.3 *Nf1*-deficient IF/+ mammary adipocytes mimic a preadipocyte and fibroblast-like cell state

Another reported phenotype of CAAs is their ability to dedifferentiate to a preadipocyte- and fibroblast-like cell through a process called adipocyte mesenchymal transition (AMT) (Dirat et al., 2011; Zhang et al., 2012; Bochet et al., 2013; Zhu et al., 2022). To determine if AMT was present in the *Nf1*-deficient IF/+ mature adipocytes, we evaluated adipocyte differentiation expression signatures. Principal component analysis (PCA) of adipocyte and fibroblast samples show that the *Nf1*-deficient IF/+ mature adipocytes cluster further away from the other *Nf1*-deficient genotypes, indicating that their gene expression profile has deviated from a typical mature adipocyte (Figure 3B). Looking at the different genes expressed at adipocyte, preadipocyte, and fibroblast stages, our RNAseq data showed the *Nf1*-deficient IF/+ mature adipocytes had lower expression of mature adipocyte markers, but higher expression of fibroblast and preadipocyte markers. WT and *Nf1*-deficient PS-20/+ and IF; PS-21/+ mature adipocytes do not have altered mesenchymal lineage gene expression. For example, adiponectin (*Adipoq*) and perilipin-1 (*Plin1*), genes which are primarily expressed in adipose tissues and mature adipocytes but are both downregulated in the IF/+ mature adipocytes. In contrast, fibroblast activation protein alpha (*Flap*) and *Cd34* are genes primarily expressed in activated fibroblast and preadipocytes, respectively, but have increased expression in the IF/+ mature adipocytes compared to the other genotypes (Figure 3A). Gene set enrichment analysis (GSEA) of the mature adipocytes revealed an enrichment in adipocyte differentiation gene signatures (obtained from the MSigDB database). To highlight one example, the *Nf1*-deficient mature adipocytes showed an enrichment in a fat cell differentiation gene set (GO0045444) which supports the difference in mesenchymal lineage markers we observed (NES = 1.29, p = 0.08; FDR = 0.024; Figure 3C). Overall, these results show that the IF/+ indel in one *Nf1* allele causes the gene expression profile of mature adipocytes before tumor formation to mimic a preadipocyte- and fibroblast-like cell state.
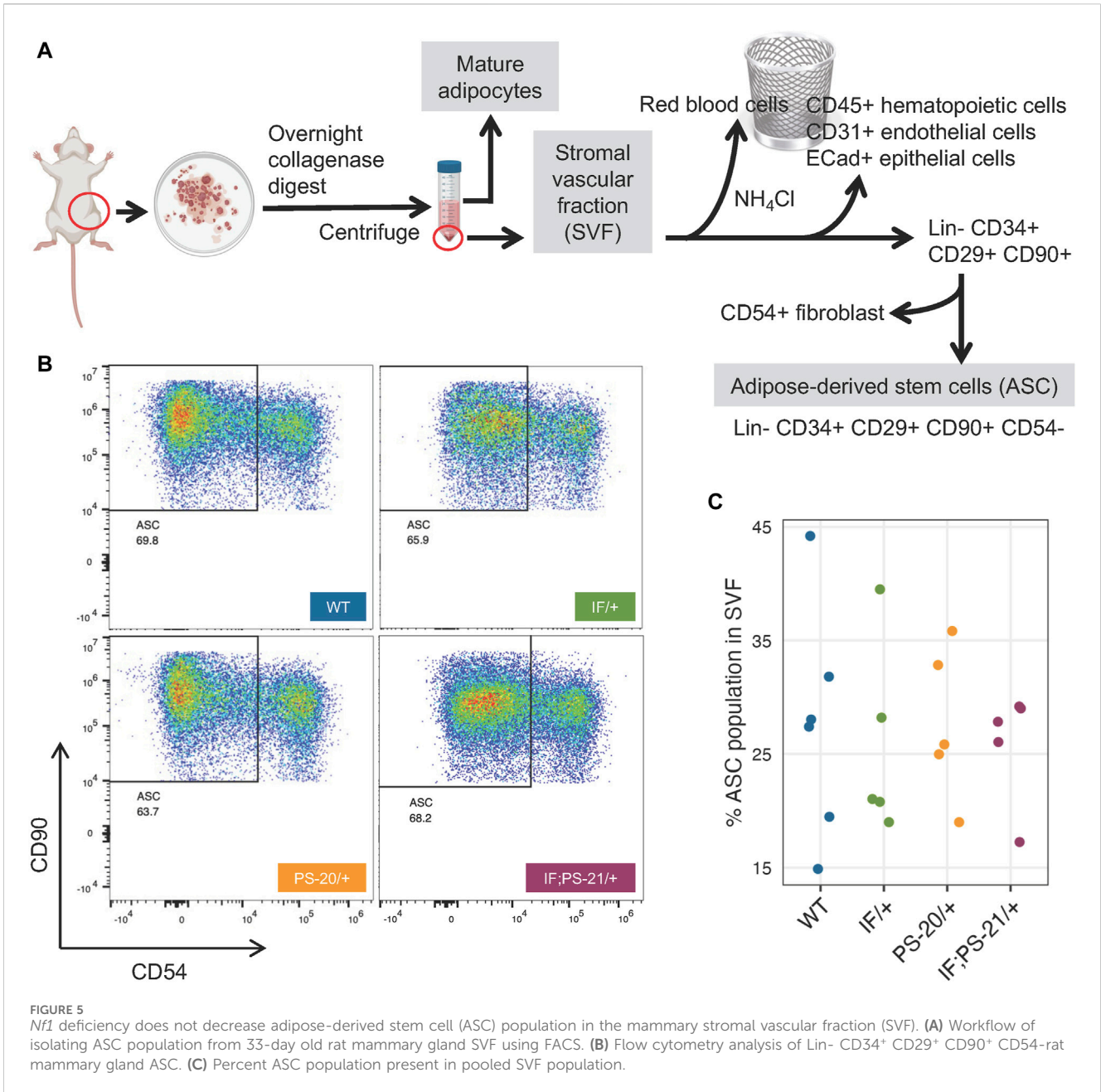
2.4 *Nf1* deficiency restricts mammary adipose-derived stem cell differentiation to immature adipocytes

To verify the altered differentiation gene expression observed in our RNAseq data (Figure 3), we isolated the adipose-derived stem

FIGURE 4
Nf1 deficiency restricts mammary adipose-derived stem cells (ASCs) differentiation to immature adipocytes. **(A)** Workflow of isolating and differentiating stromal vascular fraction (SVF) into ASCs and differentiating them further into mature adipocytes. **(B)** Brightfield images of ASC differentiation at day 5, 10, and 14, as well as Oil Red O staining at day 14. Brightfield images were acquired at 10 × magnification, scale bar is 400 μm. Oil Red O images were acquired at 4 × magnification, scale bar is 300 μm. **(C)** Quantification of cells containing lipid droplets at day 14 (WT vs. IF/+ odds ratio = 2.39, *p* = 0.08; n = 3 rats per genotype).

cell (ASC) population from 33-day-old rat mammary glands and differentiated them *in vitro* as illustrated in Figure 4A. After an overnight collagenase digest, we cultured the stromal vascular fraction (SVF) for 2-3 passages to enrich for the ASC population before culturing them in commercially available differentiation media for 2 weeks. After 2 weeks, fully differentiated cells

containing lipid droplets were counted as a measure of differentiation ability. After 14 days in differentiation media, we observed that *Nf1*-deficient IF/+ ASCs have 60% fewer cells with lipid droplets compared to WT, thus indicating a decreased differentiation ability (WT vs. IF/+ odds ratio = 0.4, *p* = 0.08; Figure 4C).

FIGURE 5
Nf1 deficiency does not decrease adipose-derived stem cell (ASC) population in the mammary stromal vascular fraction (SVF). **(A)** Workflow of isolating ASC population from 33-day old rat mammary gland SVF using FACS. **(B)** Flow cytometry analysis of Lin- CD34+ CD29+ CD90+ CD54-rat mammary gland ASC. **(C)** Percent ASC population present in pooled SVF population.

2.5 *Nf1* deficiency does not decrease adipose-derived stem cell populations in the mammary stromal vascular fraction

Mature adipocytes and preadipocytes differentiate through a multistep process originating from mesenchymal stem cells (MSCs), and in adipose tissues specifically, these tissue resident MSCs are known as ASCs (Berry and Rodeheffer, 2013; Berry et al., 2015; Brown et al., 2022). To investigate whether the reduced differentiation ability of the *Nf1*-deficient IF/+ ASC that we observed (Figure 4) was due to a decreased ASC population, we used flow cytometry to quantify the amount of ASC present in the SVF of our rat mammary glands (Figure 5A). After red blood cell removal, we derived a lineage-negative population by eliminating CD45+ hematopoietic cells, CD31+ endothelial cells, and E-Cad + epithelial cells. Using three stem cell markers, CD34+ CD29+ CD90+, we further stratified the ASC population, before excluding CD54+ fibroblasts (Rodeheffer et al., 2008; Berry and Rodeheffer, 2013; Berry et al., 2015; Jeffery et al., 2015; Jeffery et al., 2016). The abundance of the resulting ASC population (Lin- CD34+ CD29+ CD90+ CD54−) was measured compared to the whole SVF population. Even though substantial heterogeneity of ASC was observed within the genotypes, we did not detect a decrease of the Lin- CD34+ CD29+ CD90+ CD54− ASC population in *Nf1*-deficient IF/+ rats compared to WT (Figures 5B, C). Together, our differentiation assays and flow cytometry analysis indicate that *Nf1*-deficient IF/+ adipocytes have impaired differentiation that is not due to a decrease in the adipocyte progenitor population. In addition to demonstrating that *Nf1* does not impact the early stages of differentiation, these data suggest a potential of *Nf1* regulating

the later stages of adipocyte differentiation instead, specifically through PPARγ signaling.

3 Discussion

Recent breast cancer studies have highlighted the important role that *NF1* dysregulation has in both *NF1*-related and sporadic breast cancers with the focus being on epithelial cells (Zheng et al., 2020; Tovar et al., 2022). With the goal of uncovering non-epithelial contributions to NF1-related breast cancer tumorigenesis, we measured alterations in the *Nf1*-deficient mammary stromal region before tumor formation. Here we show for the first time that *Nf1*-deficiency impacts mammary stroma and the extracellular matrix, especially collagen formation, before mammary tumor formation. In the field of NF1 research, studies evaluating collagen in NF1-mediated tumorigenesis have only been conducted in the context of skin wound healing and neurofibromas (Peltonen et al., 1986; Atit et al., 1999; Brosseau et al., 2021; Kershner et al., 2022). Intriguingly, the increased expression of collagen during wound healing in mouse dermal fibroblasts with *Nf1* mutation is distinct from fibroblast collagen abnormalities due to RAS activation (Atit et al., 1999). Additionally, upregulation of protumorigenic collagen expression in *Nf1* neurofibroma fibroblasts has been recently discovered using single cell RNA sequencing (Brosseau et al., 2021; Kershner et al., 2022). Despite the known impact of collagen in breast cancer as well as other NF1-related tumors, the contribution of collagen in NF1-associated breast cancer has not been characterized. The findings in the study demonstrate that *Nf1*-deficient rats with the earliest tumor onset have a significant increase in collagen expression compared to the *Nf1*-deficient rats with later tumor onset. Notably, these collagen and matrix changes were observed weeks before tumor formation typically occurs in these *Nf1*-deficient glands. These results indicate that increased collagen deposition by *Nf1*-deficient stromal cells is associated with earlier tumor development.
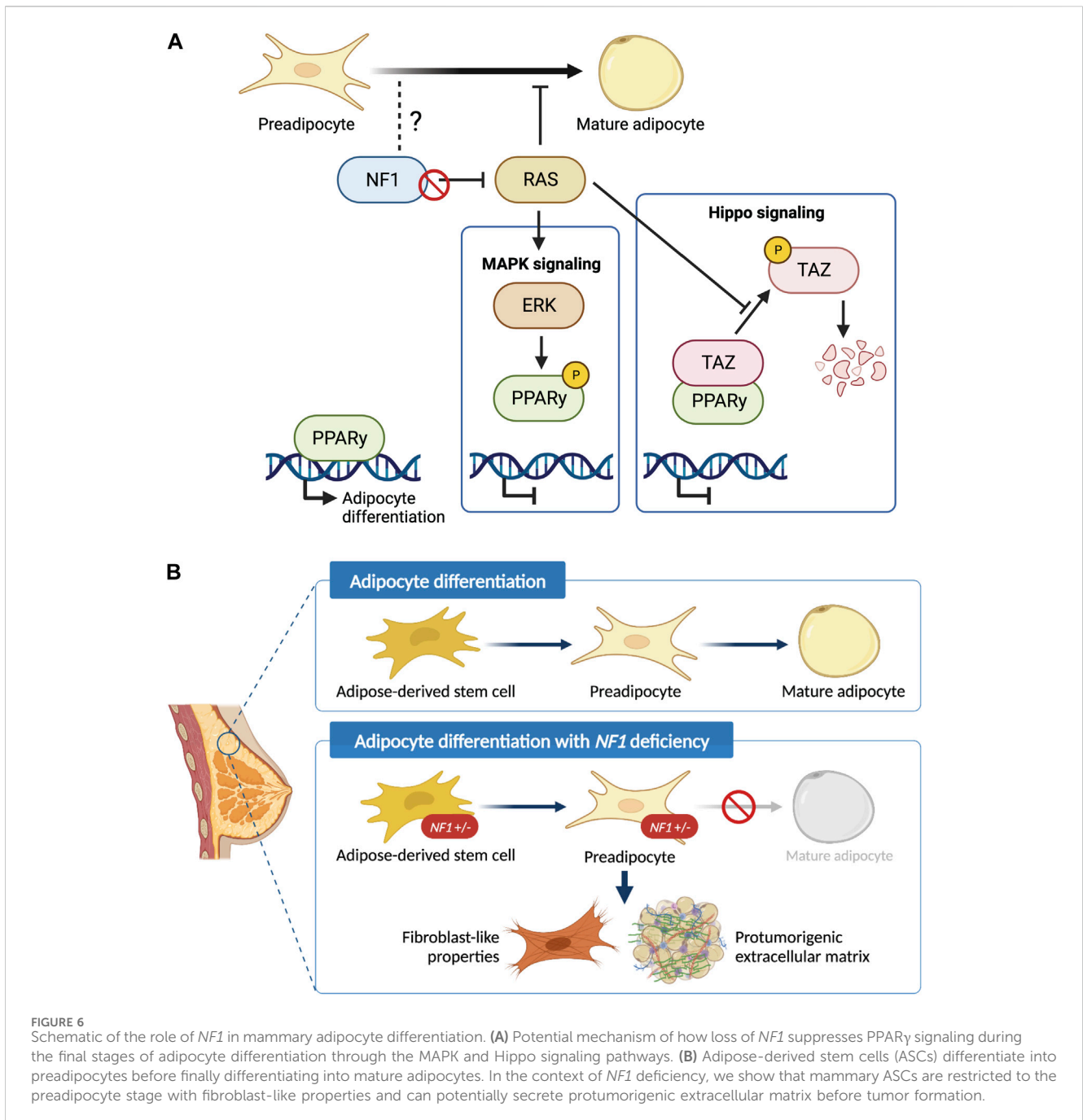
Next, we evaluated which stromal populations were driving altered matrix deposition in the pretumorigenic Nf1-deficient mammary glands. Our initial assumption was that fibroblasts were the predominant cell responsible for increasing matrix deposition, but RNAseq data led us to focus on the mammary adipocytes. Interestingly, the RNAseq analysis revealed that *Nf1*-deficient IF/+ adipocytes before tumor formation express more collagen and collagen modification genes, which are commonly associated as a feature of fibroblasts. Pathway enrichment analysis identified pathways involved in MAPK signaling, ECM deposition, and adipocyte differentiation. Additionally, *Nf1*-deficient adipocytes have a fibroblast- and preadipocyte-like expression profile and decreased expression of mature adipocyte markers. To determine if *Nf1* loss was impacting adipocyte differentiation, we isolated ASCs from the SVF population of rat mammary gland before tumor formation and observed decreased differentiation of *Nf1*-deficient IF/+ ASCs; however, flow cytometry analysis demonstrated that the abrogated differentiation was not due to a decrease in the Lin- CD34^{+} CD29^{+} CD90^{+} CD54^{−} ASC population. These results indicate that this *Nf1* loss of function promotes a preadipocyte-like phenotype, but this cell state change does not originate in the ASC population.

In addition to identifying a role for *Nf1* in promoting adipocyte plasticity, these findings also uncover important questions regarding *Nf1* loss in breast cancer initiation. The most crucial question is why

AMT only observed in mature adipocytes from *Nf1*-deficient IF/+ that have the slowest tumor onset (compared to PS-20/+ and IF; PS-21/+ *Nf1*-deficient lines). There are several potential explanations for this distinct stromal phenotype. First, we may be missing the short window of the tumor microenvironmental alterations that occur in the rapid tumor onset that occur in *Nf1*-deficient PS-20/+ and IF; PS-21/+ glands. Alternatively, these distinct stromal differences may be due to distinct signaling changes present in the IF/+ indel (only impacting the CSRD domain) compared to the premature stop indels in the rapid tumor lines. This difference indicates that *Nf1* has cell-specific functions and potentially different corresponding signaling mechanisms.

While our work and other studies have shown that the epithelial transformation is in part due to the NF1 corepressor function of ERα (Zheng et al., 2020), it is unclear whether NF1-ER signaling impacts adipocyte differentiation to promote a protumorigenic environment. Our *Nf1*-deficient models have both altered ER and RAS signaling (Dischinger et al., 2018). There are several studies elucidating the role of RAS in regulating PPARγ activity that can be applicable in the context of *NF1* deficiency (Figure 6A). PPARγ is the master regulator of adipocyte differentiation (Siersbaek et al., 2014) and is required for mature adipocytes to fully differentiate and maintain their differentiated state (Wu et al., 1999; Rosen et al., 2002; Park et al., 2012). The RAS effector ERK has been shown to phosphorylate PPARγ at Ser112 and consequently suppress PPARγ transcriptional activity (Shao et al., 1998; Choi et al., 2015). Concurrently, inhibition of KRAS has also been shown to promote *in vitro* adipogenic differentiation in the 3T3-L1 and C2C12 preadipocyte cell lines (Yu et al., 2021). Alternatively, RAS can indirectly suppress PPARγ activity through TAZ, the main downstream effector protein of the Hippo pathway. In its active state, TAZ is a transcriptional regulator that binds to PPARγ and prevents DNA binding; but in its inactive state, TAZ is phosphorylated and undergoes proteasomal degradation (Hiemer and Varelas, 2013). RAS can prevent phosphorylation and degradation of TAZ, thus suppressing adipocyte differentiation (Hong et al., 2014). Interestingly, a recent study also demonstrated that TAZ binding to PPARγ is increased with ERK-mediated phosphorylation of PPARγ at Ser112. Therefore, loss of NF1 function may impact adipocyte differentiation through RAS, PPARγ, and Hippo signaling alterations (El Ouarrat et al., 2020). Importantly, the lack of change in ASC abundance, implies that NF1 may modulate later stages of adipocyte differentiation through PPARγ. Our future studies into these signaling mechanisms will provide vital insights into adipocyte plasticity not only in breast cancer, but also in ovarian cancer which is another cancer that occurs in an adipose-rich organ and is also highly prevalent among NF1 patients (Landry et al., 2021).

In summary, findings presented in study have uncovered the previously unknown role of *Nf1* in regulating mammary collagen deposition and adipocyte plasticity (Figure 6B). These newly characterized roles of *Nf1* bring us closer to answering the clinically relevant question of why NF1 patients have an increased risk of developing breast cancer with poorer prognosis compared to the general population. Understanding the impact of adipocyte plasticity in breast cancer will allow us to identify potential vulnerabilities that can be leveraged for breast cancer early detection and treatment (Horsley, 2022; Tu and Karnoub, 2022). Additionally,

FIGURE 6
Schematic of the role of *NF1* in mammary adipocyte differentiation. **(A)** Potential mechanism of how loss of *NF1* suppresses PPARγ signaling during the final stages of adipocyte differentiation through the MAPK and Hippo signaling pathways. **(B)** Adipose-derived stem cells (ASCs) differentiate into preadipocytes before finally differentiating into mature adipocytes. In the context of *NF1* deficiency, we show that mammary ASCs are restricted to the preadipocyte stage with fibroblast-like properties and can potentially secrete protumorigenic extracellular matrix before tumor formation.

it also creates exciting new research questions regarding the signaling mechanism of *NF1* in distinct cell types as well as other aspects of adipose-related symptom manifestation in individuals with NF1.

4 Methods and materials

4.1 Animals

Female and male immunocompetent *Nf1*-deficient Sprague Dawley rats were bred in-house at the Van Andel Research Institute. The four genotypes include WT, and three *Nf1*-deficient lines: IF/+, PS-20/+, and IF; PS-21/+. Male *Nf1*-deficient rats were bred to wild-type female rats and female pups were used at the indicated developmental time-point. Animals were housed two to a cage, had *ad libitum* access to food and water, and were kept under a 12 h light - 12 h dark cycle. All animal protocols were approved by the Van Andel Research Institute Animal Care and Use Committee.

4.2 Tissue histological processing

Mammary tissues were formalin fixed and paraffin embedded utilizing routine histological procedures. Sections for H&E staining

were cut at 5 µm thickness and was performed by Van Andel Institute Pathology and Biorepository Core using a Leica Rotary microtome. Staining was performed on the Tissue-Tek Prisma Plus autostainer, using the Sakura H&E Kit #1. Slides were scanned at ×20 magnification on either a Leica Aperio XT or a Leica Aperio AT2 scanning system by the Van Andel Institute Pathology and Biorepository Core.

4.3 H&E collagen area analysis

The H&E collagen area analysis was conducted by Van Andel Institute Optical Imaging Core. Full resolution svs images of H&E-stained mammary tissue sections were imported into QuPath (version 0.4.2) for analysis (Bankhead et al., 2017). QuPath's Estimate Stain Vector tool was used to automatically deconvolve the H&E stain color vectors for each section. A region of interest (ROI) contouring the mammary gland and excluding large blood vessels and lymph nodes was manually generated for each tissue section. A pixel classifier was then created using QuPath's Pixel Classifier Tool to measure the collagen within the mammary gland ROI. The pixel classifier used an eosin stain-based threshold of 0.05, pixel resolution of 1.0062 um (equivalent to a two factor down sample), and Gaussian blur of 1.5; positive pixels were converted into an area measurement within QuPath. The areas of the mammary gland contours and pixel classifier measurements were exported into a csv file for further statistical analysis.

4.4 Picrosirius red (PSR) staining

Picrosirius red (PSR) staining was conducted by Van Andel Institute Pathology and Biorepository Core using a standard protocol (Dolber and Spach, 1987). Briefly, tissue sections 5-µm-thick tissue sections were deparaffinized, treated with phosphomolybdic acid before staining with Sirius red. Slides were washed in hydrochloric acid and 70% EtOH before cover slipping for polarized light imaging.

4.5 Polarized light microscopy

Polarized light images were acquired by Van Andel Institute Optical Imaging Core on a Zeiss AxioScan 7, using an EC Plan-Neofluar 20x/0.5 N.A. Pol M27 air objective, and ZEN Blue software (version 3.7). Tissues were illuminated with a Colibri 7 TL LED light source, imaged in brightfield at 5% intensity and 200 µs exposure, and by circularly polarized light at 10% intensity and 3.78 m exposure, sequentially. Samples were detected by an AxioCam705 color CMOS camera with 5-megapixel resolution. Resulting images were 24 bits and at 0.173×0.173 um scaling per pixel.

4.6 PSR polarized light analysis

Full resolution czi images of polarized light collected from picrosirius red-stained mammary tissue sections were imported into QuPath for analysis by Van Andel Institute Optical Imaging

Core. A ROI contouring the full tissue section was manually drawn for each slide. A pixel classifier was created using QuPath's Pixel Classifier Tool to measure the area covered by the signal from polarized light within the ROI. A training image was created from 12 equal sized rectangular regions from three different sections using QuPath's create training image tool. This resulting training image was annotated for examples of signals from the polarized light (n = 53) and background (n = 33) and used for training the pixel classifier using an artificial neural network at 1.38 µm/pixel resolution. All other settings in the pixel classifier were left at their default options. The trained pixel classifier was applied to the ROIs of all images to segment the total area covered by the polarized light signal. The segmented areas were exported from QuPath into a csv file for further statistical analysis.

4.7 Mammary fat pad digestion

Freshly isolated fourth mammary fat pads (MFP) were digested into a single cell suspension as described in Dischinger *et al.* (2018) and Tovar *et al.* (2020). Briefly, the fourth mammary fat pads from female rats are removed and digested overnight. Mature adipocytes are present in the top lipid layer and are carefully collected for RNA extraction. Red blood cells are depleted by centrifugation and lysis, respectively. The remaining cells are negatively selected using Miltenyi CD31 and CD45 biotin conjugated antibodies. Next, addition of Miltenyi anti-biotin microbeads allows capture of the antibody tagged lineage positive populations on an LS column with a Miltenyi QuadroMACS magnet. The eluted mammary epithelial cells (MECs) and fibroblasts are cultured in ultra-low attachment (ULA) plates for 48 h to deplete fibroblasts and isolate only MECs. Alternatively, to deplete MECs and isolate only fibroblast, cell pellets are cultured using differential attachment method or with fibroblast media containing gentamicin.

4.8 RNA extraction

For RNA extraction of whole fat pads and tumors, fresh harvested samples were cut up and added to MPbio lysing matrix E tube. Cells were homogenized for 20 s in an MPbio homogenizer, then RNA was isolated from the supernatant using the Trizol-chloroform-isopropanol RNA extraction method. For RNA extraction of mature adipocytes, RNA was isolated using the Trizol-chloroform-isopropanol RNA extraction method. For RNA extraction from cultured epithelial cells and fibroblast, 1.2×10^5 cells were plated into one well of a six-well plate. At 90%–100% confluency, RNA was isolated using QIAGEN QIAshredder (QIAGEN #79654) and RNeasy Kit (QIAGEN #74104) manufacturer's instructions.

4.9 Construction and sequencing of directional mRNA-seq libraries

Libraries were prepared by the Van Andel Institute Genomics Core from 500 ng of total RNA using the KAPA mRNA Hyperprep

kit (v4.17) (Kapa Biosystems, Wilmington, MA United States). RNA was sheared to 300–400 bp. Prior to PCR amplification, cDNA fragments were ligated to IDT for Illumina TruSeq UD Indexed adapters (Illumina Inc., San Diego CA, United States). Quality and quantity of the finished libraries were assessed using a combination of Agilent DNA High Sensitivity chip (Agilent Technologies, Inc.), QuantiFluor® dsDNA System (Promega Corp., Madison, WI, United States), and Kapa Illumina Library Quantification qPCR assays (Kapa Biosystems). Individually indexed libraries were pooled and 50 bp, paired-end sequencing was performed on an Illumina NovaSeq6000 sequencer using an S2 sequencing kit (Illumina Inc., San Diego, CA, United States) to an average depth of 45M reads per sample. Base calling was done by Illumina RTA3 and output of NCS was demultiplexed and converted to FastQ format with Illumina Bcl2fastq v1.9.0.

4.10 RNA sequencing data analysis

Raw reads were first trimmed of adapters with Trim_Galore (https://www.bioinformatics.babraham.ac.uk/projects/trim_galore/) and then mapped to Rnor 6.0 assembly with STAR v2.5.2b using options "--twopassMode Basic" and "--quantMode GeneCounts" to directly output counts for all features from the ensemble annotation 6. 0.90 (Dobin et al., 2013). A negative binomial generalized log-linear model was then fit to the filtered count data with edgeR using the weighted trimmed mean of M-values to normalize for library size and composition biases (Robinson et al., 2010). Different genotype or tissue groups were contrasted, and p-values were generated using empirical Bayes quasi-likelihood F-tests, and then adjusted using the BH method; adjusted p-values less than 0.05 were considered significant. Heatmaps were generated from library-size normalized counts centered across genes (z-scores) using the R package ComplexHeatmap (Gu et al., 2016). Using the normalized counts per million, the fold change against matched genotype normal mammary gland expression was calculated for tumor samples and shown as log2 (fold change) capped at −3 and 3.

4.11 Gene ontology (GO) and gene set enrichment analysis (GSEA)

The gene ontology (GO) functional enrichment analysis was performed using g:Profiler (version e106_e.g.,53_p16_65fcd97) with g:SCS multiple testing correction method applying significance threshold of $q < 0.05$ (Raudvere et al., 2019). Results were plotted using ggplot2 (v3.3.6) (Wickham, 2016). For GSEA, protein-coding genes were first pre-ranked by fold change of mutant vs. WT and loaded onto GSEA v4.3.2 (Subramanian et al., 2005). Analysis was performed on adipocyte differentiation gene signatures obtained from the MSigDB database (Liberzon et al., 2011; Liberzon et al., 2015).

4.12 SVF and ASC isolation

SVF isolation was adapted from Picon-Ruiz *et al.* (2020). After mammary fat pad digestion and red blood cell removal as described above, the SVF fraction was washed with PBS, filtered through a 70-μm cell strainer, resuspended, and plated at 3×10^5 cells/cm². After 2-3 passages in DMEM supplemented with 10% FBS and 1% penicillin/streptomycin, the cells remaining in culture were taken as the ASC population.

4.13 ASC differentiation

Adipogenic differentiation was induced using Human MesenCult™ Adipogenic Differentiation Kit (STEMCELL Technologies #05412). According to manufacturer's protocol, DMEM media was replaced with differentiation media once the ASC culture reached 90%–100% confluency. ASC culture was differentiated for 14 days with media changes every 3 days before they were used for downstream applications.

4.14 Oil red O staining

After 14 days in adipogenic differentiation media, cells were stained with Oil Red O following a standard histological protocol (Suvarna et al., 2019). Briefly, cells were fixed with 4% paraformaldehyde for 1 h at room temperature, then incubated with 60% isopropanol for 5 min before staining with Oil Red O (Sigma-Aldrich #O0625) for 30 min. After staining, cells were washed with distilled water, stained with Hematoxylin (Vector Laboratories #H-3401) for 1 min and finally washed with tap water for bluing before visualization/imaging.

4.15 Flow cytometry analysis and sorting of mammary SVF

For flow cytometry analysis, 1×10^6 cells in 100 μL were stained for 30 min at room temperature using the following antibodies: CD90-BUV395 (BD, #740260, 0.1 mg/μL), ECAD-AF405 (Novus Bio, #NBP2-98433AF405, 1.74 mg/μL), CD45-BV605 (BD, #740371, 0.4 mg/μL), CD29-SB702 (Thermo, #67–0291–82, 0.1 mg/μL), CD34 (Thermo, #PA5-47849, 1 mg/μL) with secondary AF488 (Thermo, #A-11015, 1 mg/μL), CD24-PE (Thermo, #562104, 0.2 mg/μL), CD54-R718 (BD, #751649, 0.1 mg/μL), CD140a-APC (BD, #568234, 0.2 mg/μL), and CD31-PECy7 (Thermo, #25–0310–82, 0.025 mg/μL). All fluorescence minus one (FMO) and single stain controls were stained in HF buffer (HBBS 1X with calcium chloride and magnesium chloride, supplemented with 2% FBS and 1% Pen/Step). Full panel staining was done with HF buffer and 10 μL Brilliant Stain Buffer Plus (BD Horizon #566385) per sample. Finally, cells were washed, stained with 0.005 μg/mL DAPI, filtered, and acquired on the Cytek Biosciences Aurora spectral flow cytometer by the Van Andel Institute Flow Cytometry Core. Data was analyzed using FlowJo v10.8.1. For *in vitro* phenotypic validation, cells were similarly stained and then sorted on the BD FACSymphony S6. Sorted cells were cultured in DMEM with 10% FBS and 1% Pen/Strep.

4.16 Statistical analysis

4.16.1 H&E images eosin quantification

For the day 21 data, we used a mixed-effects beta regression model from the glmmTMB package (Brooks et al., 2017) adjusted for stainer and the scanner types. We also included a random intercept for each unique image. Comparisons between genotypes were performed using emmeans (Lenth, 2022). Comparisons are given on the log-odds ratio scale or odds ratio scale and have been adjusted for multiple comparisons using the *dunnettx* method. For the day 33 data, we used a mixed-effects beta regression model from the glmmTMB package (Brooks et al., 2017) that included a random intercept for each unique image. The model was adjusted for the scanner type. There was perfect separation of the stainer and scanner types in the day 33 data, so only one of these variables was used in our models. Comparisons between genotypes were performed using emmeans (Lenth, 2022). Comparisons are given on the log-odds ratio scale or odds ratio scale and have been adjusted for multiple comparisons using the *dunnettx* method. All analyses were conducted using R v4.1.0 (https://cran.r-project.org/) with an assumed level of significant of $\alpha = 0.05$.

4.16.2 PSR-POL light quantification

A beta regression model adjusted using Tukey method for multiple comparisons was used to estimate percent of polarized light signals in all samples. To compare percent polarized light in *Nf1*-deficient genotypes to the WT, we used emmeans (Lenth, 2022). Results are given on the log odds ratio scale.

4.16.3 ASC differentiation

We used negative binomial mixed effects models with random intercepts for each animal, to estimate and compare the number of cells with lipid droplets against the WT. Tests are performed on the log scale and results are reported on the odds ratio scale.

Data availability statement

The datasets presented in this study can be found in online repositories. The names of the repository/repositories and accession number(s) can be found below: https://www.ncbi.nlm.nih.gov/, GSE231603.

Ethics statement

The animal study was approved by Van Andel Institue Institutional Animal Care and Use Committee (IACUC). The study was conducted in accordance with the local legislation and institutional requirements.

Author contributions

MA: Conceptualization, Data curation, Formal Analysis, Investigation, Methodology, Validation, Writing–original draft, Writing–review and editing. ET: Investigation, Methodology, Writing–original draft, Writing–review and editing. CE: Investigation, Methodology, Writing–original draft, Writing–review and editing. PD: Investigation, Methodology, Writing–original draft, Writing–review and editing. IB: Formal Analysis, Visualization, Writing–original draft, Writing–review and editing. EW: Formal Analysis, Visualization, Writing–original draft, Writing–review and editing. ZM: Formal Analysis, Visualization, Writing–original draft, Writing–review and editing. LT: Data curation, Methodology, Writing–original draft, Writing–review and editing. KF: Data curation, Methodology, Writing–original draft, Writing–review and editing. KG: Data curation, Formal Analysis, Methodology, Writing–original draft, Writing–review and editing. LC: Data curation, Methodology, Visualization, Writing–original draft, Writing–review and editing. MN: Data curation, Formal Analysis, Methodology, Writing–original draft, Writing–review and editing. RS: Data curation, Formal Analysis, Methodology, Writing–original draft, Writing–review and editing. CE: Methodology, Resources, Writing–original draft, Writing–review and editing. GM: Methodology, Resources, Writing–original draft, Writing–review and editing. CG: Conceptualization, Funding acquisition, Project administration, Supervision, Writing–original draft, Writing–review and editing. MS: Conceptualization, Funding acquisition, Project administration, Resources, Supervision, Writing–original draft, Writing–review and editing.

Conflict of interest

The authors declare that the research was conducted in the absence of any commercial or financial relationships that could be construed as a potential conflict of interest.

Publisher's note

All claims expressed in this article are solely those of the authors and do not necessarily represent those of their affiliated organizations, or those of the publisher, the editors and the reviewers. Any product that may be evaluated in this article, or claim that may be made by its manufacturer, is not guaranteed or endorsed by the publisher.

Supplementary material

The Supplementary Material for this article can be found online at: https://www.frontiersin.org/articles/10.3389/fcell.2024.1375441/full#supplementary-material

References

(2012). Comprehensive molecular portraits of human breast tumours. *Nature* 490 (7418), 61–70. doi:10.1038/nature11412

Atit, R. P., Crowe, M. J., Greenhalgh, D. G., Wenstrup, R. J., and Ratner, N. (1999). The Nf1 tumor suppressor regulates mouse skin wound healing, fibroblast proliferation, and collagen deposited by fibroblasts. *J. Investig. Dermatol.* 112 (6), 835–842. doi:10.1046/j.1523-1747.1999.00609.x

Attane, C., and Muller, C. (2020). Drilling for Oil: tumor-surrounding adipocytes fueling cancer. *Trends Cancer* 6 (7), 593–604. doi:10.1016/j.trecan.2020.03.001

Bainer, R., Frankenberger, C., Rabe, D., An, G., Gilad, Y., and Rosner, M. R. (2016). Gene expression in local stroma reflects breast tumor states and predicts patient outcome. *Sci. Rep.* 6, 39240. doi:10.1038/srep39240

Bankhead, P., Loughrey, M. B., Fernandez, J. A., Dombrowski, Y., McArt, D. G., Dunne, P. D., et al. (2017). QuPath: open source software for digital pathology image analysis. *Sci. Rep.* 7 (1), 16878. doi:10.1038/s41598-017-17204-5

Berry, R., and Rodeheffer, M. S. (2013). Characterization of the adipocyte cellular lineage *in vivo*. *Nat. Cell. Biol.* 15 (3), 302–308. doi:10.1038/ncb2696

Berry, R., Rodeheffer, M. S., Rosen, C. J., and Horowitz, M. C. (2015). Adipose tissue residing progenitors adipocyte lineage progenitors and adipose derived stem cells ADSC. *Curr. Mol. Biol. Rep.* 1 (3), 101–109. doi:10.1007/s40610-015-0018-y

Bertucci, F., Ng, C. K. Y., Patsouris, A., Droin, N., Piscuoglio, S., Carbuccia, N., et al. (2019). Genomic characterization of metastatic breast cancers. *Nature* 569 (7757), 560–564. doi:10.1038/s41586-019-1056-z

Bi, P., Yue, F., Karki, A., Castro, B., Wirbisky, S. E., Wang, C., et al. (2016). Notch activation drives adipocyte dedifferentiation and tumorigenic transformation in mice. *J. Exp. Med.* 213 (10), 2019–2037. doi:10.1084/jem.20160157

Bochet, L., Lehuede, C., Dauvillier, S., Wang, Y. Y., Dirat, B., Laurent, V., et al. (2013). Adipocyte-derived fibroblasts promote tumor progression and contribute to the desmoplastic reaction in breast cancer. *Cancer Res.* 73 (18), 5657–5668. doi:10.1158/0008-5472.CAN-13-0530

Brooks, M. E., Kristensen, K., Benthem, K.Jv, Magnusson, A., Berg, C. W., Nielsen, A., et al. (2017). glmmTMB balances speed and flexibility among packages for zero-inflated generalized linear mixed modeling. *R J.* 9 (2), 378. doi:10.32614/rj-2017-066

Brosseau, J. P., Sathe, A. A., Wang, Y., Nguyen, T., Glass, D. A., 2nd, Xing, C., et al. (2021). Human cutaneous neurofibroma matrisome revealed by single-cell RNA sequencing. *Acta Neuropathol. Commun.* 9 (1), 11. doi:10.1186/s40478-020-01103-4

Brown, A. C. (2022). "Insights into the adipose stem cell niche in health and disease," in *Scientific principles of adipose stem cells*. Editors L. Kokai, K. Marra, and J. P. Rubin (Germany: Academic Press), 57–80.

Choi, S., Jung, J. E., Yang, Y. R., Kim, E. S., Jang, H. J., Kim, E. K., et al. (2015). Novel phosphorylation of PPARγ ameliorates obesity-induced adipose tissue inflammation and improves insulin sensitivity. *Cell. Signal* 27 (12), 2488–2495. doi:10.1016/j.cellsig.2015.09.009

Coelho, P. G. B., Souza, M. V., Conceicao, L. G., Viloria, M. I. V., and Bedoya, S. A. O. (2018). Evaluation of dermal collagen stained with picrosirius red and examined under polarized light microscopy. *Bras Dermatol* 93 (3), 415–418. doi:10.1590/abd1806-4841.20187544

Curran, C. S., and Ponik, S. M. (2022). *The mammary tumor microenvironment*, 163–181. 12962020.

Daly, M. B., Pilarski, R., Berry, M., Buys, S. S., Farmer, M., Friedman, S., et al. (2017). NCCN guidelines insights: genetic/familial high-risk assessment: breast and ovarian, version 2.2017. *J. Natl. Compr. Canc Netw.* 15 (1), 9–20. doi:10.6004/jnccn.2017.0003

de Visser, K. E., and Joyce, J. A. (2023). The evolving tumor microenvironment: from cancer initiation to metastatic outgrowth. *Cancer Cell.* 41 (3), 374–403. doi:10.1016/j.ccell.2023.02.016

Dirat, B., Bochet, L., Dabek, M., Daviaud, D., Dauvillier, S., Majed, B., et al. (2011). Cancer-associated adipocytes exhibit an activated phenotype and contribute to breast cancer invasion. *Cancer Res.* 71 (7), 2455–2465. doi:10.1158/0008-5472.CAN-10-3323

Dischinger, P. S., Tovar, E. A., Essenburg, C. J., Madaj, Z. B., Gardner, E. E., Callaghan, M. E., et al. (2018). NF1 deficiency correlates with estrogen receptor signaling and diminished survival in breast cancer. *NPJ Breast Cancer* 4, 29. doi:10.1038/s41523-018-0080-8

Dobin, A., Davis, C. A., Schlesinger, F., Drenkow, J., Zaleski, C., Jha, S., et al. (2013). STAR: ultrafast universal RNA-seq aligner. *Bioinformatics* 29 (1), 15–21. doi:10.1093/bioinformatics/bts635

Dolber, P. C., and Spach, M. S. (1987). Picrosirius red staining of cardiac muscle following phosphomolybdic acid treatment. *Stain Technol.* 62 (1), 23–26. doi:10.3109/10520298709107961

El Ouarrat, D., Isaac, R., Lee, Y. S., Oh, D. Y., Wollam, J., Lackey, D., et al. (2020). TAZ is a negative regulator of PPARγ activity in adipocytes and TAZ deletion improves insulin sensitivity and glucose tolerance. *Cell. Metab.* 31 (1), 162–173.e5. doi:10.1016/j.cmet.2019.10.003

Evans, D. G., Howard, E., Giblin, C., Clancy, T., Spencer, H., Huson, S. M., et al. (2010). Birth incidence and prevalence of tumor-prone syndromes: estimates from a UK family genetic register service. *Am. J. Med. Genet. A* 152A (2), 327–332. doi:10.1002/ajmg.a.33139

Finak, G., Bertos, N., Pepin, F., Sadekova, S., Souleimanova, M., Zhao, H., et al. (2008). Stromal gene expression predicts clinical outcome in breast cancer. *Nat. Med.* 14 (5), 518–527. doi:10.1038/nm1764

Griffiths, S., Thompson, P., Frayling, I., and Upadhyaya, M. (2007). Molecular diagnosis of neurofibromatosis type 1: 2 years experience. *Fam. Cancer* 6 (1), 21–34. doi:10.1007/s10689-006-9001-3

Gu, Z., Eils, R., and Schlesner, M. (2016). Complex heatmaps reveal patterns and correlations in multidimensional genomic data. *Bioinformatics* 32 (18), 2847–2849. doi:10.1093/bioinformatics/btw313

Hiemer, S. E., and Varelas, X. (2013). Stem cell regulation by the Hippo pathway. *Biochim. Biophys. Acta* 1830 (2), 2323–2334. doi:10.1016/j.bbagen.2012.07.005

Hong, X., Nguyen, H. T., Chen, Q., Zhang, R., Hagman, Z., Voorhoeve, P. M., et al. (2014). Opposing activities of the Ras and Hippo pathways converge on regulation of YAP protein turnover. *EMBO J.* 33 (21), 2447–2457. doi:10.15252/embj.201489385

Horsley, V. (2022). Adipocyte plasticity in tissue regeneration, repair, and disease. *Curr. Opin. Genet. Dev.* 76, 101968. doi:10.1016/j.gde.2022.101968

Jeffery, E., Church, C. D., Holtrup, B., Colman, L., and Rodeheffer, M. S. (2015). Rapid depot-specific activation of adipocyte precursor cells at the onset of obesity. *Nat. Cell. Biol.* 17 (4), 376–385. doi:10.1038/ncb3122

Jeffery, E., Wing, A., Holtrup, B., Sebo, Z., Kaplan, J. L., Saavedra-Pena, R., et al. (2016). The adipose tissue microenvironment regulates depot-specific adipogenesis in obesity. *Cell. Metab.* 24 (1), 142–150. doi:10.1016/j.cmet.2016.05.012

Kershner, L. J., Choi, K., Wu, J., Zhang, X., Perrino, M., Salomonis, N., et al. (2022). Multiple Nf1 Schwann cell populations reprogram the plexiform neurofibroma tumor microenvironment. *JCI Insight* 7 (18), e154513. doi:10.1172/jci.insight.154513

Koczkowska, M., Callens, T., Chen, Y., Gomes, A., Hicks, A. D., Sharp, A., et al. (2020). Clinical spectrum of individuals with pathogenic NF1 missense variants affecting p.Met1149, p.Arg1276, and p.Lys1423: genotype-phenotype study in neurofibromatosis type 1. *Hum. Mutat.* 41 (1), 299–315. doi:10.1002/humu.23929

Koczkowska, M., Chen, Y., Callens, T., Gomes, A., Sharp, A., Johnson, S., et al. (2018). Genotype-phenotype correlation in NF1: evidence for a more severe phenotype associated with missense mutations affecting NF1 codons 844-848. *Am. J. Hum. Genet.* 102 (1), 69–87. doi:10.1016/j.ajhg.2017.12.001

Lammert, M., Friedman, J. M., Kluwe, L., and Mautner, V. F. (2005). Prevalence of neurofibromatosis 1 in German children at elementary school enrollment. *Arch. Dermatol* 141 (1), 71–74. doi:10.1001/archderm.141.1.71

Landry, J. P., Schertz, K. L., Chiang, Y. J., Bhalla, A. D., Yi, M., Keung, E. Z., et al. (2021). Comparison of cancer prevalence in patients with neurofibromatosis type 1 at an academic cancer center vs in the general population from 1985 to 2020. *JAMA Netw. Open* 4 (3), e210945. doi:10.1001/jamanetworkopen.2021.0945

Lenth, R. V. (2022). Emmeans: estimated marginal means, aka least-squares means. *R. package version 1.8.0.*, 2022. Available at: https://CRAN.R-project.org/package=emmeans.

Liberzon, A., Birger, C., Thorvaldsdottir, H., Ghandi, M., Mesirov, J. P., and Tamayo, P. (2015). The Molecular Signatures Database (MSigDB) hallmark gene set collection. *Cell. Syst.* 1 (6), 417–425. doi:10.1016/j.cels.2015.12.004

Liberzon, A., Subramanian, A., Pinchback, R., Thorvaldsdottir, H., Tamayo, P., and Mesirov, J. P. (2011). Molecular signatures database (MSigDB) 3.0. *Bioinformatics* 27 (12), 1739–1740. doi:10.1093/bioinformatics/btr260

Lupton, C. J., Bayly-Jones, C., D'Andrea, L., Huang, C., Schittenhelm, R. B., Venugopal, H., et al. (2021). The cryo-EM structure of the human neurofibromin dimer reveals the molecular basis for neurofibromatosis type 1. *Nat. Struct. Mol. Biol.* 28 (12), 982–988. doi:10.1038/s41594-021-00687-2

Madanikia, S. A., Bergner, A., Ye, X., and Blakeley, J. O. (2012). Increased risk of breast cancer in women with NF1. *Am. J. Med. Genet. A* 158A (12), 3056–3060. doi:10.1002/ajmg.a.35550

Meric-Bernstam, F., Frampton, G. M., Ferrer-Lozano, J., Yelensky, R., Perez-Fidalgo, J. A., Wang, Y., et al. (2014). Concordance of genomic alterations between primary and recurrent breast cancer. *Mol. Cancer Ther.* 13 (5), 1382–1389. doi:10.1158/1535-7163.MCT-13-0482

Mo, J., Moye, S. L., McKay, R. M., and Le, L. Q. (2022). Neurofibromin and suppression of tumorigenesis: beyond the GAP. *Oncogene* 41 (9), 1235–1251. doi:10.1038/s41388-021-02156-y

Mukherjee, A., Bilecz, A. J., and Lengyel, E. (2022). The adipocyte microenvironment and cancer. *Cancer Metastasis Rev.* 41 (3), 575–587. doi:10.1007/s10555-022-10059-x

Myllyharju, J., and Kivirikko, K. I. (2004). Collagens, modifying enzymes and their mutations in humans, flies and worms. *Trends Genet.* 20 (1), 33–43. doi:10.1016/j.tig.2003.11.004

Nee, K., Ma, D., Nguyen, Q. H., Pein, M., Pervolarakis, N., Insua-Rodriguez, J., et al. (2023). Preneoplastic stromal cells promote BRCA1-mediated breast tumorigenesis. *Nat. Genet.* 55 (4), 595–606. doi:10.1038/s41588-023-01298-x

Oh, E. Y., Christensen, S. M., Ghanta, S., Jeong, J. C., Bucur, O., Glass, B., et al. (2015). Extensive rewiring of epithelial-stromal co-expression networks in breast cancer. *Genome Biol.* 16 (1), 128. doi:10.1186/s13059-015-0675-4

Park, B. O., Ahrends, R., and Teruel, M. N. (2012). Consecutive positive feedback loops create a bistable switch that controls preadipocyte-to-adipocyte conversion. *Cell. Rep.* 2 (4), 976–990. doi:10.1016/j.celrep.2012.08.038

Pearson, A., Proszek, P., Pascual, J., Fribbens, C., Shamsher, M. K., Kingston, B., et al. (2020). Inactivating NF1 mutations are enriched in advanced breast cancer and contribute to endocrine therapy resistance. *Clin. Cancer Res.* 26 (3), 608–622. doi:10.1158/1078-0432.CCR-18-4044

Peltonen, J., Penttinen, R., Larjava, H., and Aho, H. J. (1986). Collagens in neurofibromas and neurofibroma cell cultures. *Ann. N. Y. Acad. Sci.* 486, 260–270. doi:10.1111/j.1749-6632.1986.tb48079.x

Rasmussen, S. A., and Friedman, J. M. (2000). NF1 gene and neurofibromatosis 1. *Am. J. Epidemiol.* 151 (1), 33–40. doi:10.1093/oxfordjournals.aje.a010118

Ratner, N., and Miller, S. J. (2015). A RASopathy gene commonly mutated in cancer: the neurofibromatosis type 1 tumour suppressor. *Nat. Rev. Cancer* 15 (5), 290–301. doi:10.1038/nrc3911

Raudvere, U., Kolberg, L., Kuzmin, I., Arak, T., Adler, P., Peterson, H., et al. (2019). g: Profiler: a web server for functional enrichment analysis and conversions of gene lists (2019 update). *Nucleic Acids Res.* 47 (W1), W191-W198–W8. doi:10.1093/nar/gkz369

Razavi, P., Chang, M. T., Xu, G., Bandlamudi, C., Ross, D. S., Vasan, N., et al. (2018). The genomic landscape of endocrine-resistant advanced breast cancers. *Cancer Cell.* 34 (3), 427–438. doi:10.1016/j.ccell.2018.08.008

Robinson, M. D., McCarthy, D. J., and Smyth, G. K. (2010). edgeR: a Bioconductor package for differential expression analysis of digital gene expression data. *Bioinformatics* 26 (1), 139–140. doi:10.1093/bioinformatics/btp616

Rodeheffer, M. S., Birsoy, K., and Friedman, J. M. (2008). Identification of white adipocyte progenitor cells *in vivo*. *Cell.* 135 (2), 240–249. doi:10.1016/j.cell.2008.09.036

Rosen, E. D., Hsu, C. H., Wang, X., Sakai, S., Freeman, M. W., Gonzalez, F. J., et al. (2002). C/EBPalpha induces adipogenesis through PPARgamma: a unified pathway. *Genes. Dev.* 16 (1), 22–26. doi:10.1101/gad.948702

Seminog, O. O., and Goldacre, M. J. (2015). Age-specific risk of breast cancer in women with neurofibromatosis type 1. *Br. J. Cancer* 112 (9), 1546–1548. doi:10.1038/bjc.2015.78

Shao, D., Rangwala, S. M., Bailey, S. T., Krakow, S. L., Reginato, M. J., and Lazar, M. A. (1998). Interdomain communication regulating ligand binding by PPAR-gamma. *Nature* 396 (6709), 377–380. doi:10.1038/24634

Sharif, S., Moran, A., Huson, S. M., Iddenden, R., Shenton, A., Howard, E., et al. (2007). Women with neurofibromatosis 1 are at a moderately increased risk of developing breast cancer and should be considered for early screening. *J. Med. Genet.* 44 (8), 481–484. doi:10.1136/jmg.2007.049346

Siersbaek, R., Rabiee, A., Nielsen, R., Sidoli, S., Traynor, S., Loft, A., et al. (2014). Transcription factor cooperativity in early adipogenic hotspots and super-enhancers. *Cell. Rep.* 7 (5), 1443–1455. doi:10.1016/j.celrep.2014.04.042

Sokol, E. S., Feng, Y. X., Jin, D. X., Basudan, A., Lee, A. V., Atkinson, J. M., et al. (2019). Loss of function of NF1 is a mechanism of acquired resistance to endocrine therapy in lobular breast cancer. *Ann. Oncol.* 30 (1), 115–123. doi:10.1093/annonc/mdy497

Stephens, P. J., Tarpey, P. S., Davies, H., Van Loo, P., Greenman, C., Wedge, D. C., et al. (2012). The landscape of cancer genes and mutational processes in breast cancer. *Nature* 486 (7403), 400–404. doi:10.1038/nature11017

Subramanian, A., Tamayo, P., Mootha, V. K., Mukherjee, S., Ebert, B. L., Gillette, M. A., et al. (2005). Gene set enrichment analysis: a knowledge-based approach for interpreting genome-wide expression profiles. *Proc. Natl. Acad. Sci. U. S. A.* 102 (43), 15545–15550. doi:10.1073/pnas.0506580102

Suvarna, K. L., Christopher, B., and John, D. (2019). *Bancroft's theory and practice of histological techniques*. Eighth ed. USA: Elsevier, 557.

Tovar, E. A., Arumugam, M., Essenburg, C. J., Dischinger, P. S., Grit, J. L., Callaghan, M. E., et al. (2022). Nf1 deficiency accelerates mammary development and promotes luminal-basal plasticity. *bioRxiv*. doi:10.1101/2022.12.22.520633

Tu, Z., and Karnoub, A. E. (2022). Mesenchymal stem/stromal cells in breast cancer development and management. *Semin. Cancer Biol.* 86 (Pt 2), 81–92. doi:10.1016/j.semcancer.2022.09.002

Uusitalo, E., Kallionpaa, R. A., Kurki, S., Rantanen, M., Pitkaniemi, J., Kronqvist, P., et al. (2017). Breast cancer in neurofibromatosis type 1: overrepresentation of unfavourable prognostic factors. *Br. J. Cancer* 116 (2), 211–217. doi:10.1038/bjc.2016.403

Uusitalo, E., Rantanen, M., Kallionpaa, R. A., Poyhonen, M., Leppavirta, J., Yla-Outinen, H., et al. (2016). Distinctive cancer associations in patients with neurofibromatosis type 1. *J. Clin. Oncol.* 34 (17), 1978–1986. doi:10.1200/JCO.2015.65.3576

Wang, X., Levin, A. M., Smolinski, S. E., Vigneau, F. D., Levin, N. K., and Tainsky, M. A. (2012). Breast cancer and other neoplasms in women with neurofibromatosis type 1: a retrospective review of cases in the Detroit metropolitan area. *Am. J. Med. Genet. A* 158A (12), 3061–3064. doi:10.1002/ajmg.a.35560

Wang, Y. Y., Valet, P., Muller, C., Wang, Y. Y., Attané, C., Milhas, D., et al. (2017). Mammary adipocytes stimulate breast cancer invasion through metabolic remodeling of tumor cells. *JCI insight* 2 (4), 874899–e87521. doi:10.1172/jci.insight.87489

Wei, X., Li, S., He, J., Du, H., Liu, Y., Yu, W., et al. (2019). Tumor-secreted PAI-1 promotes breast cancer metastasis via the induction of adipocyte-derived collagen remodeling. *Cell. Commun. Signal* 17 (1), 58. doi:10.1186/s12964-019-0373-z

Wickham, H. (2016). *ggplot2: elegant graphics for data analysis*. Germany: Springer-Verlag New York.

Wu, C., Dong, S., Huang, R., and Chen, X. (2023). Cancer-associated adipocytes and breast cancer: intertwining in the tumor microenvironment and challenges for cancer therapy. *Cancers (Basel)* 15 (3), 726. doi:10.3390/cancers15030726

Wu, Z., Rosen, E. D., Brun, R., Hauser, S., Adelmant, G., Troy, A. E., et al. (1999). Cross-regulation of C/EBP alpha and PPAR gamma controls the transcriptional pathway of adipogenesis and insulin sensitivity. *Mol. Cell.* 3 (2), 151–158. doi:10.1016/s1097-2765(00)80306-8

Xu, G. F., O'Connell, P., Viskochil, D., Cawthon, R., Robertson, M., Culver, M., et al. (1990). The neurofibromatosis type 1 gene encodes a protein related to GAP. *Cell.* 62 (3), 599–608. doi:10.1016/0092-8674(90)90024-9

Yap, Y. S., McPherson, J. R., Ong, C. K., Rozen, S. G., Teh, B. T., Lee, A. S., et al. (2014). The NF1 gene revisited - from bench to bedside. *Oncotarget* 5 (15), 5873–5892. doi:10.18632/oncotarget.2194

Yates, L. R., Knappskog, S., Wedge, D., Farmery, J. H. R., Gonzalez, S., Martincorena, I., et al. (2017). Genomic evolution of breast cancer metastasis and relapse. *Cancer Cell.* 32 (2), 169–184. doi:10.1016/j.ccell.2017.07.005

Young, L. C., Goldstein de Salazar, R., Han, S. W., Huang, Z. Y. S., Merk, A., Drew, M., et al. (2023). Destabilizing NF1 variants act in a dominant negative manner through neurofibromin dimerization. *Proc. Natl. Acad. Sci. U. S. A.* 120 (5), e2208960120. doi:10.1073/pnas.2208960120

Yu, W., Chen, C. Z., Peng, Y., Li, Z., Gao, Y., Liang, S., et al. (2021). KRAS affects adipogenic differentiation by regulating autophagy and MAPK activation in 3T3-L1 and C2C12 cells. *Int. J. Mol. Sci.* 22 (24), 13630–13718. doi:10.3390/ijms222413630

Zhang, Y., Daquinag, A. C., Amaya-Manzanares, F., Sirin, O., Tseng, C., and Kolonin, M. G. (2012). Stromal progenitor cells from endogenous adipose tissue contribute to pericytes and adipocytes that populate the tumor microenvironment. *Cancer Res.* 72 (20), 5198–5208. doi:10.1158/0008-5472.CAN-12-0294

Zheng, Z. Y., Anurag, M., Lei, J. T., Cao, J., Singh, P., Peng, J., et al. (2020). Neurofibromin is an estrogen receptor-α transcriptional Co-repressor in breast cancer. *Cancer Cell.* 37 (3), 387–402 e7. doi:10.1016/j.ccell.2020.02.003

Zhu, Q., Zhu, Y., Hepler, C., Zhang, Q., Park, J., Gliniak, C., et al. (2022). Adipocyte mesenchymal transition contributes to mammary tumor progression. *Cell. Rep.* 40 (11), 111362. doi:10.1016/j.celrep.2022.111362